JACS
JOURNAL OF THE AMERICAN CHEMICAL SOCIETY
Article
pubs.acs.org/JACS

The Interplay of Al and Mg Speciation in Advanced Mg Battery Electrolyte Solutions

Kimberly A. See,[†] Karena W. Chapman,[*,‡] Lingyang Zhu,[†] Kamila M. Wiaderek,[‡] Olaf J. Borkiewicz,[‡] Christopher J. Barile,[†] Peter J. Chupas,[‡] and Andrew A. Gewirth[*,†]

[†]Department of Chemistry, University of Illinois at Urbana−Champaign, Urbana, Illinois 61801, United States
[‡]X-ray Science Division, Advanced Photon Source, Argonne National Laboratory, Argonne, Illinois 60439, United States

Supporting Information

ABSTRACT: Mg batteries are an attractive alternative to Li-based energy storage due to the possibility of higher volumetric capacities with the added advantage of using sustainable materials. A promising emerging electrolyte for Mg batteries is the magnesium aluminum chloride complex (MACC) which shows high Mg electrodeposition and stripping efficiencies and relatively high anodic stabilities. As prepared, MACC is inactive with respect to Mg deposition; however, efficient Mg electrodeposition can be achieved following an electrolytic conditioning process. Through the use of Raman spectroscopy, surface enhanced Raman spectroscopy, ^{27}Al and ^{35}Cl nuclear magnetic resonance spectroscopy, and pair distribution function analysis, we explore the active vs inactive complexes in the MACC electrolyte and demonstrate the codependence of Al and Mg speciation. These techniques report on significant changes occurring in the bulk speciation of the conditioned electrolyte relative to the as-prepared solution. Analysis shows that the active Mg complex in conditioned MACC is very likely the $[Mg_2(\mu\text{−}Cl)_3\cdot 6THF]^+$ complex that is observed in the solid state structure. Additionally, conditioning creates free Cl^- in the electrolyte solution, and we suggest the free Cl^- adsorbs at the electrode surface to enhance Mg electrodeposition.

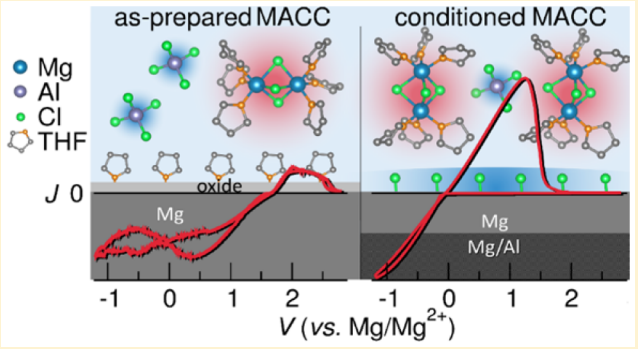

INTRODUCTION

Mg batteries are an attractive alternative to Li-based energy storage.[1] The biggest advantage of Mg is the potential to achieve larger energy densities compared with the conventional Li-ion battery while using abundant and inexpensive resources. The theoretical volumetric capacity of Mg metal anodes is 3833 mAh cm^{-3}, about 4.5 times larger than the ubiquitous graphite anode in a Li-ion battery. While electrodeposition of Li yields dendrites that can short circuit the battery, electrodeposition of Mg results in a relatively smooth morphology making metal anodes a viable prospect.[2,3] To realize a functioning battery with a Mg metal anode, an electrolyte system must be developed that supports Mg deposition and stripping with high Coulombic efficiencies and large current densities while utilizing safe components. These electrolyte characteristics are challenging due to the inherently high reactivity of Mg metal which precludes the use of many known aprotic battery solvents and commercially available Mg salts.

Only a handful of electrolyte families for Mg metal batteries have been identified and none are without compromise. The earliest electrolytes, based on highly reactive Grignard reagents, exhibit high Coulombic efficiencies but are unstable as evidenced by their low anodic stabilities (1.5 V vs Mg).[4] Another family of electrolytes, stemming from the Grignard paradigm, is the organohaloaluminate electrolytes.[5] Organohaloaluminates exhibit a high overpotential for electrodeposition and low anodic stability, albeit higher than the Grignards (2.5 V vs Mg for the all-phenyl complex).[6]

The use of Grignards in a battery electrolyte solution, however, is not viable for safety reasons. A few promising advanced Mg battery electrolyte solutions have been discovered that do not use Grignards including those based on the borohydride anion,[7] dicarborane anion,[8] monocarborane anion[9] and trifluoromethanesulfonyl imide anion.[10,11] A much simpler advanced electrolyte termed the magnesium aluminum chloride complex (MACC) is composed of only inorganic salts.[12] The preparation of MACC is deceivingly simple whereby $MgCl_2$ and $AlCl_3$ are dissolved at a 2:1 ratio in THF.[12] The MACC is able to support Mg deposition and stripping at high Coulombic efficiencies (99%) with an anodic stability of 3.1−3.4 V vs Mg without the use of Grignards.[12,13] The as-prepared MACC is unable to support Mg electrodeposition and requires electrolytic conditioning before the system will support reversible Mg deposition and stripping.[14] Conditioning is achieved by cycling the electrolyte with a Pt working electrode and a Mg counter/reference negative and positive of 0 V (vs Mg/Mg^{2+}) until steady-state Mg deposition and stripping behavior is achieved,

Received: October 20, 2015
Published: December 4, 2015

DOI: 10.1021/jacs.5b10987
J. Am. Chem. Soc. 2016, 138, 328−337

often after over 50 cycles. During conditioning, Al is irreversibly reduced on the working electrode and, correspondingly, the Mg:Al ratio is increased from 2:1 to 2.6:1.[14] The highly efficient Mg electrodeposition and stripping achievable with conditioned MACC is a property of the bulk electrolyte solution. Changes in the electrode surface are not the cause for enhancement because the same Coulombic efficiency and electrodeposition overpotential can be achieved with a clean Pt electrode once the electrolyte is conditioned.[14] The disadvantage of the MACC electrolyte, in addition to the energy intensive conditioning process, is its poor temporal stability. Upon resting conditioned MACC at open circuit, significant degradation is observed as evidenced by an increase in the Mg deposition overpotential, a decrease in the current density, and a decrease in the Coulombic efficiency.[14]

The need for conditioning provides an inactive electrolyte with respect to Mg electrochemical activity in the as-prepared state and an active electrolyte in the conditioned state. Here we explore the speciation and local atomic structure of the Al and Mg solute species in both the as-prepared and conditioned states, as well as the pure $AlCl_3$ and $MgCl_2$ component solutions, to identify the species active for Mg deposition and stripping. Complementary insights from bulk and surface-enhanced Raman spectroscopy (SERS), ^{27}Al and ^{35}Cl nuclear magnetic resonance (NMR) spectroscopy, and pair distribution function (PDF) analysis are applied to reveal the bulk electrolyte composition and solute speciation changes in the mixed cation MACC system. Understanding the conditioning process provides insights into the complexes responsible for Mg deposition and stripping allowing for the critical further development of MACC and next-generation electrolytes. Such an understanding will allow us to identify strategies to accelerate and improve the energy efficiency of MACC conditioning, and to possibly stabilize the conditioned MACC for longer periods.

EXPERIMENTAL SECTION

Electrolyte Preparation. The MACC electrolytes were prepared according to Barile et al.[14] All chemicals were purchased from Sigma Aldrich. THF was purchased anhydrous and further dried by refluxing under Ar over Na and benzophenone. Prior to loading into the glovebox, the THF was degassed via 3 freeze−pump−thaw cycles. Once in the glovebox, activated 3 Å molecular sieves were added and the THF was allowed to sit at least overnight prior to use. The $MgCl_2$ (Alfa Aesar) was purchased anhydrous and further dried under flowing Ar and HCl gas (about 1 L/min) for 2.5 h at 300 °C. Upon cooling, the reaction tube was filled with Ar, sealed, and brought into the glovebox. The $AlCl_3$ was purchased anhydrous and used as received. The MACC was prepared by cooling 2.5 mL of THF and $AlCl_3$ (0.020 g) with a Thermoelectrics Unlimited, Inc. TCP-2−1 cold plate (~0 °C). Once the $AlCl_3$ and THF were cooled, the THF was added dropwise to the $AlCl_3$ to minimize the formation of THF adducts and polyTHF. $MgCl_2$ (0.029 g) was added to an additional 2.5 mL of room temperature THF and stirred ($MgCl_2$ was not yet dissolved). The $AlCl_3$ solution was then added dropwise to the stirring $MgCl_2$/THF. The solution was allowed to stir for at least 6 h to yield a clear, colorless solution.

Conditioning Protocol. The MACC was conditioned with a 0.5 mm Pt wire working electrode and a Mg counter/reference. The Pt (Alfa Aesar) was cleaned in concentrated HNO_3 and heated in a H_2 flame prior to use. The Mg foil (GalliumSource, LLC) was mechanically cleaned with a razor blade in the glovebox prior to use. Electrochemical cells were assembled in an Ar glovebox with 1.0 mL of electrolyte. Electrochemistry was controlled on CH Instruments 600D, 620A, 760C, or 760D potentiostats or a SP-150 BioLogic potentiostat. All voltages are reported with respect to Mg/Mg^{2+}. The cell was conditioned using cyclic voltammetry (CV) from −1.2 to 2.8 V at 5 mV s^{-1} until reversible, steady state behavior was observed with nearly 100% Coulombic efficiency (99% being the lower limit). All characterization performed on the conditioned MACC electrolyte was performed on the electrolyte following excursion to 0 V on the negative sweep with minimal resting time.

Characterization Details. Raman spectroscopy was measured with a He/Ne laser at an excitation wavelength of 632.8 nm using an instrument described previously.[15] The resolution of the measurement was estimated to be ± 5.6−6.7 cm^{-1} with a 50 μm slit and ± 3.5−4.2 cm^{-1} with a 20 μm slit. The solutions were contained in a 1 cm × 1 cm quartz cuvette sealed with a Teflon screw cap. The solutions were excited with a laser setup previously described.[15] The signal was averaged over 240 acquisitions lasting 2 s each.

SERS was measured in a screw cap cuvette with a roughened Cu foil substrate to provide the SERS enhancement. Prior to introduction to the electrolyte, the Cu foil was etched with HNO_3 and electrochemically roughened in a 0.1 M KCl aqueous solution with a Ag/AgCl (no leak, Cypress) reference electrode and a Cu counter electrode. The Cu foil was cycled 15 times from 0.44 V (vs Ag/AgCl) to − 0.96 V (vs Ag/AgCl) at 0.1 V s^{-1} with a potential hold at the low potential cutoff for 10 s. The Cu foil was then rinsed with copious amounts of Milli Q water followed by isopropanol and then immediately placed in the glovebox antechamber. The Cu foil was dried under dynamic vacuum overnight.

^{27}Al NMR spectroscopy was performed on a 600 MHz Varian instrument in 5 mm screw cap NMR tubes in the University of Illinois at Urbana−Champaign School of Chemical Sciences NMR laboratory. External standards were introduced within each sample tube via sealed capillaries containing $Al(NO_3)_3$ in D_2O. The ^{27}Al NMR was measured with a 90 degree pulse width of 9.95 μs, an acquisition time of 0.2 s, and a relaxation delay of 0.5 s. ^{35}Cl NMR was performed on a 750 MHz Agilent instrument also in the UIUC SCS NMR laboratory in 5 mm screw cap NMR tubes. The ^{35}Cl NMR was measured with a 90 degree pulse width of 29.8 μs, acquisition time of 0.15 s, and relaxation delay of 0.15 s. The spectra were collected for at least 1.5 h to achieve good signal-to-noise.

The X-ray total scattering data suitable for PDF analysis were collected at beamline 11-ID-B at the Advanced Photon Source[16,17] (λ = 0.2114 Å) for solutions sealed in 3-mm diameter glass tubes. The PDF for the solutions were obtained following correction for Compton scattering, detector effects and background scattering measured for the empty sealed tube, Fourier transforming the reduced structure factor to Q_{max} = 20 $Å^{-1}$, in PDFgetX2[18] as previously described.[17]

RESULTS AND DISCUSSION

We first discuss the evolution of Mg electrodeposition and stripping during the conditioning process of the MACC electrolyte to place the as-prepared and conditioned states in context. The first conditioning cycle is dominated by irreversible Al electrodeposition (Figure 1a) as evidenced by the cathodic activity starting around 1.6 V (E^0 $Al^{3+/0}$ = 0.7 V vs $Mg^{2+/0}$).[14] We suggest that Al-related electrochemistry is active in this region as prior work found Al deposition occurred on the working electrode.[14] The oxidative feature at potentials positive of 1.6 V is likely associated with either a decomposition process or Al oxidation. Al electrodeposition is gradually replaced by Mg deposition and stripping behavior (Figure 1b) and the Mg contribution to the current response increases in later cycles (Figure 1c). Eventually, steady-state behavior showing the electrodeposition and stripping of Mg is achieved (Figure 1d). The evolution in Mg stripping and deposition voltammetry with cycle number shows that the Mg activity in the as-prepared state is starkly different from that in the conditioned state. We now introduce Raman, NMR, and X-ray PDF characterization of these two states—along with the

DOI: 10.1021/jacs.5b10987
J. Am. Chem. Soc. 2016, 138, 328−337

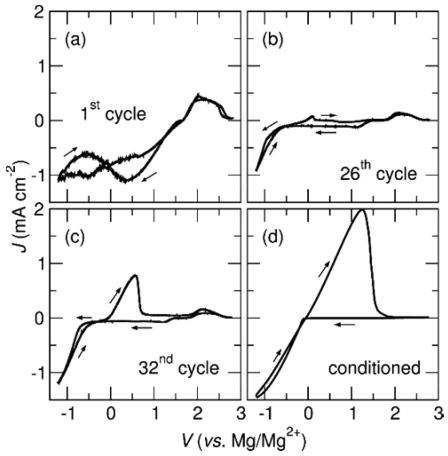

Figure 1. Electrochemical evolution of 0.06 M $MgCl_2$ + 0.03 M $AlCl_3$ in THF (MACC) as it conditions. (a) The first cycle is dominated by Al electrochemistry. (b) Intermediate cycles start to show the evolution of Mg deposition and stripping which (c) continue to become more pronounced. (d) The conditioned electrolyte shows reversible Mg deposition and stripping at nearly 100% Coulombic efficiency. The MACC is conditioned with a Pt working electrode and a Mg counter/reference at 5 mV s^{-1} from − 1.2 to 2.8 V.

constituent starting materials to understand the conditioning process and identify the active complexes.

Raman Spectroscopy Results. Figure 2 shows the Raman spectra obtained from the MACC electrolyte constituents as

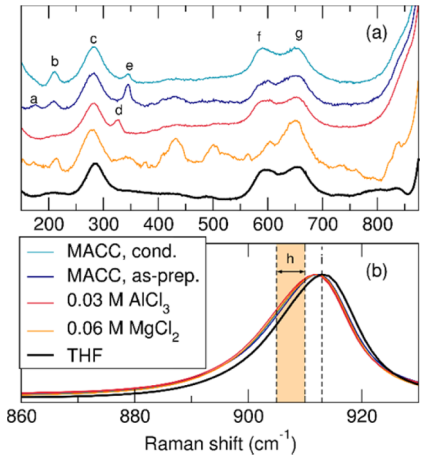

Figure 2. Raman spectra of the MACC electrolyte (as-prepared and conditioned) along with the component solutions collected with a 10 μm entrance slit and a 632.8 nm excitation. (a) A new peak is observed at 207 cm^{-1} in the conditioned electrolyte likely due to Mg species supporting reversible Mg reduction and stripping. (b) The symmetric stretching of the $-CH_2-$ moieties α to the ether O shifts to lower wavenumbers in the MACC electrolyte solutions suggesting an elongation of the ether linkage likely due to coordination to a cationic center. Tabulated assignments can be found in Table 1.

well as the as-prepared and conditioned MACC. Table 1 provides band assignments. The spectra of the electrolyte and its components are dominated by THF modes (peaks c, f, g, h, and i). The $MgCl_2$ component solution exhibits a large number of modes, suggesting that the solution is heterogeneous, likely due to the poor solubility of anhydrous $MgCl_2$ in THF.[19] The Mg−Cl stretching is observed at 212 cm^{-1} consistent with previous reports of $MgCl_2$ coordinated by THF.[5,6] Additional species in the spectrum are difficult to identify, however, and the multitude of peaks suggests species are present due to various changes in coordination by THF and disproportionation of the Mg moieties.

In contrast, the $AlCl_3$ component solution exhibits only one prominent mode at 325 cm^{-1} assigned to neutral $AlCl_3$ coordinated by THF.[6] The modes expected for other possible Al species, including the tetrahedral $AlCl_4^-$ and THF adducts, are not observed. This analysis is confirmed by the ^{27}Al NMR data (vide infra). THF adducts of Al are not observed in the Raman spectrum despite the strong Lewis acidity of $AlCl_3$ toward THF due to the low temperature preparation method which is intended to minimize such products.

The Raman spectrum of the as-prepared MACC exhibits both new and persisting modes compared to the spectra of the two component solutions. The Mg−Cl stretching mode is again observed at 211 cm^{-1}. However, the other modes indicative of heterogeneity are absent, suggesting that the presence of the Al changes Mg speciation. The speciation of the Al shifts from the neutral species in the component solution, to anionic $AlCl_4^-$ as evidenced by the fundamental modes commonly ascribed to $AlCl_4^-$ at 175 cm^{-1} and 211 cm^{-1} (modes a and e, respectively).[6] $Al_2Cl_7^-$, expected at 394 cm^{-1},[20,21] is not observed in the Raman. The formation of the $AlCl_4^-$ again confirms that the addition of $MgCl_2$ to the solution affects the speciation of the Al. We note that $MgCl_2$ solubility is greatly enhanced in the presence of $AlCl_3$, likely due to the formation of ionic complexes. This change in Al speciation also allows for Al deposition during the initial cycles when conditioning the MACC. Additionally, speciation of Al in $AlCl_3$/THF solutions is strongly dependent on concentration.[22] Therefore, as Al is gradually irreversibly deposited during conditioning, it is very likely that the decrease in concentration of Al also contributes to a change in speciation which eventually favors an electrochemically inert Al complex.

The conditioned MACC displays a slightly different Raman spectrum compared to the as-prepared solution. Mode b, assigned to $MgCl_2$, increases in intensity while the $AlCl_3$ modes, a and e, decrease significantly. The poor Coulombic efficiencies observed in the early conditioning cycles indicate that Al deposition is largely irreversible and thus Al is gradually removed from the electrolyte as conditioning progresses, causing the Al modes to decrease in intensity. The lower $AlCl_4^-$ concentration is also confirmed by ^{27}Al NMR (vide infra). The high intensity of peak b in the conditioned MACC compared with the Mg-Cl mode in the $MgCl_2$ component solution could be due to an increase in the concentration of Mg−Cl-containing complexes. An increase in Mg^{2+} concentration may result from Mg oxidation at the counter electrode. Another possible cause for the increase in intensity of mode b is the formation of a complex with enhanced Raman cross section. One such species could be the $[Mg_2(\mu\text{-}Cl)_3]^+$ dimer species that is observed in the solid state structure of the crystallized MACC.[13]

The THF modes also provide insight into the structure of the solvated complexes. The most intense THF mode, observed around 915 cm^{-1} (Figure 2b), is made up of two modes (bands h and i) attributed to C−C stretching (~910 cm^{-1}) and C−O stretching (~913 cm^{-1}).[27] THF coordination to cations through the ether O causes mode h to red shift[22,27,28] making this mode a good indicator of THF complexation.[29,30] Figure 2b shows that in solutions containing cationic centers, mode h is indeed red-shifted compared to pure THF suggesting

DOI: 10.1021/jacs.5b10987
J. Am. Chem. Soc. 2016, 138, 328−337

Table 1. Assignments of Raman Shifts for Peaks in the MACC and Its Component Solutions

	Raman shift (cm^{-1})					assignment		
peak ID	THF	$MgCl_2$	$AlCl_3$	MACC, as-prep.	MACC, cond.	species	mode(s)	ref.
a				176		$AlCl_4^-$	F_2 bending	6,22
b		214		211	208	Mg−Cl	A_1	5,6,23
c	283	279	282	281	280	THF	βCX_2 (bend + rock) + ring pucker	24,25
d			325			$AlCl_3$·2THF	Al−Cl	6,26
e				344	344	$AlCl_4^-$	A_1 symmetric stretching	6,22
f	599	594	588	592	592	THF	αCH_2 (bend + twist) + $C_\alpha C_\beta$ asym. stretch + ring pucker	24,25
g	655	650	654	653	650	THF	αCH_2 (bend + twist + rock) + βCH_2 (twist + rock) + ring bend	24,25
h	910	905	908	908	908	THF	βCH_2 (wag + twist) + COC sym. stretch + $C_\beta C_\beta$ stretch	24,25
i	913	913	913	913	913	THF	$C_\alpha C_\beta$ sym. stretch + αCH_2 (wag + twist) + βCH_2 (wag + bend)	24,25

THF ligation in all cases. The ubiquitous presence of THF-cation coordination is likely the origin of the strong sensitively of the Mg deposition electrochemistry on the solvent.[31]

The Raman spectra begin to explain the species formed in the MACC electrolyte. The $AlCl_3$ solution is composed of neutral $AlCl_3$·2THF while the $MgCl_2$ solution is extremely heterogeneous and difficult to characterize. In the as-prepared MACC, the $MgCl_2$ solubility is enhanced via the formation of ions in solution including $AlCl_4^-$ that must be counterbalanced by Mg cationic complexes containing Mg−Cl. Upon conditioning, the Mg−Cl associated stretches gain intensity suggesting either an increase in the concentration of Mg−Cl bonds, or a change in the Mg coordination to produce a structure with a higher Raman cross section. Additionally, the $AlCl_4^-$ intensity in the conditioned electrolyte decreases relative to the as-prepared solution due to irreversible Al plating occurring in the first conditioning cycles.

SERS was measured on a roughened Cu substrate to probe complexes at the electrode interface and obtain insight into deposition mechanisms. Cu was chosen as the SERS substrate due to the well-characterized enhancement of Cu−Cl stretches at the surface. The Cu−Cl stretch is expected at 300 cm^{-1} for free Cl^- adsorbed at the Cu surface.[32−34] Figure 3 shows the SERS spectra of the as-prepared, conditioned, and aged conditioned MACC. A strong Cu−Cl stretch is observed at 300 cm^{-1} due to a Cl decorated Cu surface. The Cu−Cl mode is much more intense in the conditioned electrolyte relative to the as-prepared electrolyte presumably due to a change in the amount of Cl^- present on the Cu surface. Upon aging the electrolyte, the Cu−Cl mode decreases in intensity suggesting a removal of Cl^- from the surface. An additional change in the spectrum is found in mode h, around 912 cm^{-1}. The SERS spectrum of pure THF on Cu is blue-shifted relative to the normal Raman spectrum of THF an effect likely due to O coordination at the Cu surface, similar to the shift in THF modes observed in the normal Raman spectra due to cation coordination. The conditioned MACC, however, exhibits a THF mode which is red-shifted relative to the pure THF indicating negligible THF coordination to the Cu surface. Interestingly, as the MACC begins to age, the Cu−Cl mode decreases in intensity while mode h shifts to a frequency corresponding to a condition in which THF coordination at the surface is present, essentially replacing the Cl^- decorated surface with a THF adsorbed surface. The SERS data therefore suggest that the electrochemical performance is directly correlated to the ability of Cl^- to decorate the electrode surface. If Cl^- is unavailable to coat the surface, THF coordination is instead observed. The high oxophilicity of

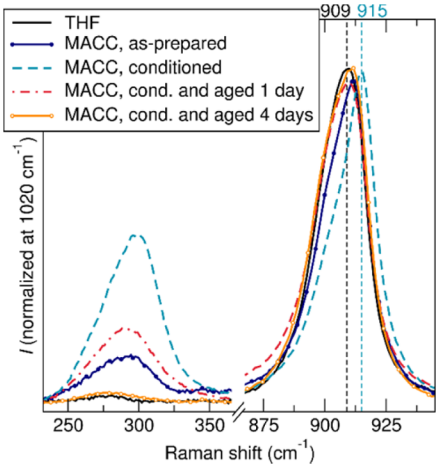

Figure 3. Surface enhanced Raman spectroscopy (SERS) of the MACC electrolyte on roughened Cu foil. All signals are normalized to a THF mode at 1020 cm^{-1} (not shown). Spectra are shown for the electrolyte as prepared and conditioned. The SERS was also measured on conditioned MACC that was allowed to age for 1−4 days. The Cu−Cl stretch is observed for the MACC electrolyte both in the as-prepared state and after conditioning at 300 cm^{-1}. If the electrolyte ages at least for 4 days, the Cu−Cl mode is no longer apparent suggesting minimal Cl^- coordination at the electrode surface. The THF mode just above 900 cm^{-1} is highly sensitive to coordination. A shift to lower frequencies is observed relative to normal Raman of THF due to coordination of THF on the Cu surface. The Raman shifts of the THF peak in the conditioned MACC and the pure THF are indicated by the vertical lines at 915 cm^{-1} and 909 cm^{-1}, respectively.

Mg[35,36] suggests that THF coordination to a Mg surface is likely very strong and thus passivates the electrode.

NMR Spectroscopy Results. Al speciation was evaluated using ^{27}Al NMR. Figure 4a shows the ^{27}Al NMR spectra of the MACC before and after conditioning along with the spectrum of the $AlCl_3$ component solution. The spectra are shown with the background signal from the probe and each individual NMR tube removed. In order to scale the background correctly, a sealed capillary standard was used to normalize the signals. Information regarding the shielding of the Al center can be deduced from the chemical shift of the resonance while the symmetry of the coordination environment can be estimated by the line broadening due to the quadrupolar nature of ^{27}Al. The $AlCl_3$ solution displays one prominent peak at 64 ppm and small contributions at 103 ppm, 39 ppm, and 12 ppm. The 64 ppm resonance is ascribed to $AlCl_3$·2THF,[37−39] which is also the only species observed in the Raman. The small 103 ppm resonance is well-known to arise from the tetrahedral $AlCl_4^-$

DOI: 10.1021/jacs.5b10987
J. Am. Chem. Soc. 2016, 138, 328−337

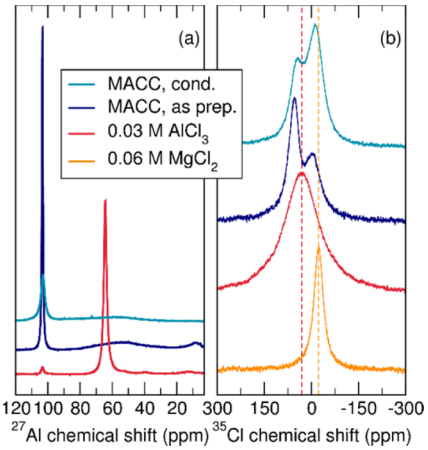

Figure 4. (a) ^{27}Al NMR spectra of the 0.03 M $AlCl_3$ component solution, as-prepared MACC, and conditioned MACC show a change in the Al speciation when the MACC is conditioned. The ^{27}Al resonances are referenced to $Al(NO_3)_3$ (0 ppm). (b) ^{35}Cl NMR spectra of as-prepared MACC, conditioned MACC, and aged MACC. The ^{35}Cl resonances are referenced to NaCl (0 ppm).

species.[26,40] The $AlCl_4^-$ is charge balanced by a cationic species observed, also with low intensity, at 12 ppm corresponding to $[AlCl_2{\cdot}4THF]^+$. ^{27}Al NMR confirms that the Al in a 0.03 M $AlCl_3$ in THF solution is mostly present as neutral $AlCl_3{\cdot}2THF$.

In contrast, Al in the as-prepared electrolyte speciates strongly toward the $AlCl_4^-$ (103 ppm) due to the addition of $MgCl_2$. This agrees well with the appearance of the $AlCl_4^-$ modes in the Raman data of as-prepared MACC and previous ^{27}Al NMR data on the as-prepared MACC.[13] The speciation of Al toward $AlCl_4^-$ likely promotes Al electrodeposition during the initial conditioning cycles. In fact, electrodeposition of Al requires plating baths with high concentrations of Cl.[41] Interestingly, other mixed cation Mg electrolytes, such as the all-phenyl complex, have not been reported to support Al electrodeposition.[42] The other reported Mg electrolytes that contain Al are prepared by reaction of a Mg Grignard with $AlCl_3$. In these cases, the speciation toward $AlCl_4^-$ is not favored and instead, Al exists mostly as AlR_4^-, AlR_3Cl^-, and $AlRCl_2^-$.[6] The organohaloaluminum complexes do not support Al electrodeposition likely due to kinetic limitations imposed by the organic ligands.[31] There remains some cationic six coordinate Al in the solution at 10 ppm and a new, very broad resonance is observed at about 50 ppm. The broad resonance at 50 ppm is likely due to a noncubic, five-coordinate Al species such as $AlCl_3{\cdot}2THF$[39] while the 10 ppm peak is due to six-coordinate $[AlCl_2{\cdot}4THF]^+$. This speciation is in contrast to that observed in the $AlCl_3$ component solution, which contains the same concentration of $AlCl_3$ as the MACC, and exhibits only minor contributions from $AlCl_4^-$. $Al_2Cl_7^-$, which would appear as a broader, more deshielded resonance compared to $AlCl_4^-$,[43] is not observed in any of the solutions. Upon conditioning, the intensity of the $AlCl_4^-$ signal in the NMR decreases significantly and the secondary species at 10 ppm disappears. The line width of the $AlCl_4^-$ resonance also increases due to the dilution of this species.[37] Interestingly, a new, sharp peak is observed at 73 ppm in the conditioned electrolyte; however, this peak is extremely small and thus represents a very minor species.

Although information regarding Mg speciation cannot be deduced directly from the ^{27}Al NMR, the ^{27}Al NMR does indeed provide further evidence that Al and Mg speciation are codependent. The ^{27}Al NMR of the as-prepared electrolyte is dominated by the anionic $AlCl_4^-$ species. Even if the remaining Al complexes are assumed to be cationic, electroneutrality cannot be achieved by considering the Al species alone since the concentration of the $AlCl_4^-$ far outweighs that of the secondary complexes. To achieve electroneutrality, therefore, the speciation of Mg must favor formation of cationic species compared to the native equilibrium in the 'single component' $MgCl_2$ solution.

Evidence for changes in the Cl environment after conditioning can be observed from ^{35}Cl NMR (Figure 4b). ^{35}Cl, like ^{27}Al, is also a quadrupolar nucleus so the signal width reports on the symmetry of the Cl environment. The $MgCl_2$ solution exhibits one strong peak at −23 ppm suggesting a single environment. The $AlCl_3$ solution exhibits one broad peak at 31 ppm, significantly shifted from the $MgCl_2$ solution likely due to the greater ability of Al^{3+} to draw electron density from the Cl ligands compared to Mg^{2+}. Due to the broad nature of the Cl peak in the $AlCl_3$ component solution, the Cl environment around Al is less symmetric compared with Mg in the component solutions.

The two resonances corresponding to Al and Mg coordination appear to be preserved in the as-prepared MACC as evidenced by two distinct resonances in the ^{35}Cl NMR (Figure 4b). Interestingly, both the high and low frequency resonances are shifted to a more deshielded frequency relative to the component solutions. Table 2 contains

Table 2. Lorentzian Fit Values of ^{35}Cl NMR

	shift (ppm)	fwhm (MHz)	relative area
0.06 M $MgCl_2$	−23	2425	100
0.03 M $AlCl_3$	31	9922	100
MACC, as-prep.	−6	2131	41
	56	3013	59
MACC, cond.	−13	3969	62
	45	3895	38

the measured shift, the full width at half-maximum (fwhm) value, and the relative percentage of each contribution as determined by fitted Lorentzian functions. Two dashed lines corresponding to the observed resonances in each component solution are included in Figure 4b to guide the eye. The shift in the Al-related Cl is due to the change in coordination from $AlCl_3{\cdot}2THF$ to $AlCl_4^-$, which results in a more deshielded Cl^- due to the lower coordination number of the Al. The high symmetry of the tetragonal $AlCl_4^-$ results in a much sharper ^{35}Cl resonance as evidenced by the decrease in the fwhm. The deshielding of the Mg-bound Cl suggests that Cl is either more tightly bound to the Mg center or the coordination geometry of the Mg complexes has changed compared to the $MgCl_2$ component solution.

The resonances of the two Cl environments in the conditioned MACC remain shifted to higher frequencies relative to the component solutions. The relative area associated with each resonance changes significantly compared to the as-prepared MACC. In the as-prepared solution, 41% of the Cl is present in the low frequency region while 59% is present in the high frequency region (as determined from the peak areas). Upon conditioning, the distribution shifts to 62% and 38% between the low and high frequency resonances, respectively. This suggests that the conditioned electrolyte

DOI: 10.1021/jacs.5b10987
J. Am. Chem. Soc. 2016, 138, 328−337

contains a higher concentration of Cl associated with Mg, which agrees well with the increase in the Mg−Cl stretching mode intensity in the Raman spectroscopy. This increase correlates with a decrease in the concentration of Cl associated with Al, again, agreeing well with the Raman data. Significantly, however, the resonance of the Cl associated with Mg in the conditioned electrolyte remains shifted to a deshielded environment compared the $MgCl_2$ component solutions.

X-ray Total Scattering Results. The X-ray total scattering data, S(Q), were measured on the electrolytes before and after conditioning to observe conditioning-associated changes in the local structure. The X-ray PDF provides detailed local structural information as a histogram of all atom-atom distances within the sample. These are weighted by the X-ray scattering power of the atoms involved. Accordingly, the data are dominated by correlations involving the more strongly scattering elements (Cl, Mg, and Al) or correlations with high multiplicity or high relative concentration. In electrolyte solutions, PDF can be applied to reveal the local coordination geometry of the ions in solution, including the distance to coordinated ions and solvent molecules, as well as any well-defined correlations beyond the first coordination sphere.

The X-ray total scattering data were collected for the pure THF solvent, component Al and Mg solutions, and MACC before and after conditioning to identify changes in the local atomic structure as a result of conditioning. The as-measured PDFs are shown in Figure 5a and are dominated by features

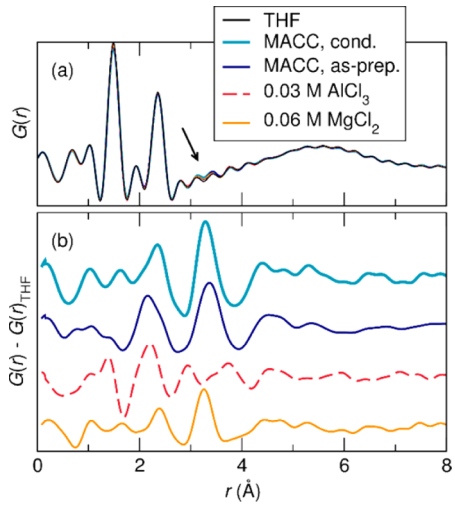

Figure 5. (a) PDF of the as-prepared and conditioned MACC electrolyte solution along with the component solutions and neat THF. (b) PDF shown with the THF correlations subtracted.

associated with the THF molecules of the solvent, which is the dominate species in these dilute solutions. The 0.03 M $AlCl_3$ solution contains only 0.5 wt % $AlCl_3$ while the 0.06 M $MgCl_2$ solution contains 0.6 wt % $MgCl_2$. Even at these low concentrations, significant differences were evident in the PDFs when comparing all the solutions, most notably centered at ∼3.3 Å (Figure 5a).

The PDF measured for pure THF was subtracted from that measured for the solutions to isolate the features associated with the solute complexes (Figure 5b). The subtracted THF PDF was normalized to eliminate the feature at ∼1.5 Å, which is unique to the C−C and C−O bonds within individual THF molecules. While features below 1.5 Å should be effectively eliminated in the differential, small features remain which suggests a change in some intramolecular THF−THF correlations in the solutions upon coordination with cationic species. This is consistent with the Raman data which suggest changes in C−O bond length within THF upon coordination.

The differential PDFs reveal notable differences in the correlations for the component Al and Mg solutions, and as-prepared and conditioned MACC (Figure 5b). Differences between the PDFs reflect significant changes in the Mg^{2+} and Al^{3+} structures not only as a consequence of the conditioning process, but also upon mixing of the cationic solutions. A linear combination of the $AlCl_3$ and $MgCl_2$ component solutions poorly describes the as-prepared MACC which further confirms the codependence of speciation for both the Mg and Al complexes. Features between ∼2−2.5 Å are likely associated with coordination bonds between the Mg^{2+} and Al^{3+} cation and solvating species. In these systems, the first shell bonds are either M−Cl or M−O due to THF coordination. Features between 3 and 4 Å likely reflect next-nearest neighbor correlations that involve either the cationic centers with next-nearest neighbors or the first shell atoms, such as Cl or O, with next-nearest neighbors.

A quantitative analysis of atom-atom correlations above 2 Å was undertaken by fitting Gaussian functions to the features in the differential PDFs. The total fit is plotted over the differential PDFs in Figure 6a. The peak center and area for each component Gaussian are plotted in Figure 6b and tabulated in Table 3. Tabulated data for correlations larger than 4.5 Å can be found in the SI.

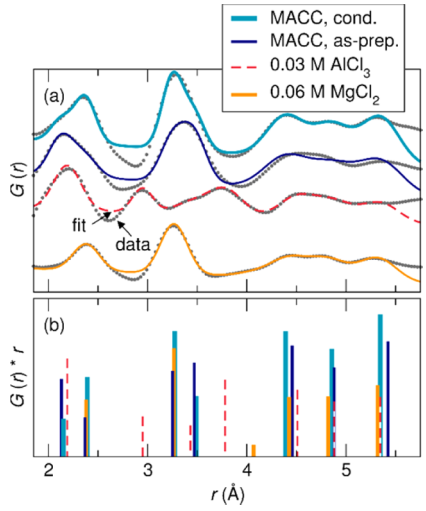

Figure 6. (a) Fits of the XPDF data for the MACC, conditioned MACC, and its component solutions. The data for each solution are shown in gray with the total fit overlaid. The total fit is comprised of several Gaussian functions and a linear background. (b) Each component Gaussian is shown for all solutions to enable direct comparison. The magnitude of the bar chart corresponds to the area of each component Gaussian.

The differential PDF for the $MgCl_2$ solution contains a single first shell correlation centered at 2.38 Å that can be attributed to Mg−Cl and/or Mg−O coordination bonds. The Mg−O and Mg−Cl bond lengths are predicted to be between 1.9−2.1 Å and 2.2−2.3 Å, respectively, by first-principles molecular dynamics simulations.[44] The measured first shell correlation is between the bond length for Mg−Cl of 2.46 Å found in solid

DOI: 10.1021/jacs.5b10987
J. Am. Chem. Soc. 2016, 138, 328−337

Table 3. Gaussian Fit Parameters of the XPDF Data

		relative area normalized to	
	peak center (Å)	Mg first shell	Al first shell
0.06 M $MgCl_2$	2.38	1	
	3.27	1.9	
	4.07	0.21	
0.03 M $AlCl_3$	2.19		1
	2.95		0.41
	3.43		0.32
	3.78		0.78
MACC, as-prep.	2.13	2	1
	2.37	1	0.50
	3.25	2.2	1.1
	3.47	2.4	1.2
MACC, cond.	2.15	0.47	1
	2.39	1	2.1
	3.27	1.6	3.3
	3.49	0.76	1.6

$MgCl_2$[45] and the Mg−O bond length of 2.10 Å in MgO.[46] Mg is octahedrally coordinated in both structures. A more intense correlation observed at 3.27 Å is attributed to next-nearest neighbor correlations. This correlation is difficult to understand due to the heterogeneity of the solution observed in the Raman spectrum. Therefore, further interpretation of the Mg coordination was not pursued.

The PDF of the $AlCl_3$ solution matches well to a neutral pentacoordinate $AlCl_3$·2THF complex, which is consistent with the ^{27}Al NMR and Raman data. The first shell correlation at 2.19 Å is associated with Al−O and Al−Cl coordination bonds. The observed first shell bond distances are similar to those measured in the solid state structure of $AlCl_3$·2THF at 1.99 Å and 2.15 Å for Al−O and Al−Cl, respectively.[47] The next correlation at 2.95 Å corresponds to Cl···O correlations found at 2.92−2.94 Å in the solid state structure.[47] The feature at 2.95 Å corresponds to Al···C correlations with the THF ligands. The feature at 3.47 Å is likely associated with correlations between the Cl ligands and the α-C in the ligated THF in the pentacoordinate species. The 3.47 Å feature could also contain contributions from the Cl···Cl correlations that would be expected for the tetrahedral $AlCl_4^-$, expected at 3.42 Å, due to the small quantity of $AlCl_4^-$ observable in the ^{27}Al NMR. The feature at 3.78 Å is associated with Cl···Cl correlations between equatorially coordinated Cl ligands at a ∼120 degree angle to the Al. Note, this Cl···Cl correlation is longer than would be expected for a tetrahedral $AlCl_4^-$ species and is thus a good indication of the pentacoordinate geometry that is implicated in the Raman and ^{27}Al NMR.

The PDF of the as-prepared MACC PDF shows a feature at 2.17 Å which is consistent with the Al−Cl distance in $AlCl_4^-$, the dominate Al species suggested by spectroscopic analyses. The feature at 2.43 Å is similar to that in the $MgCl_2$ solution and can be attributed to Mg−Cl and/or Mg−O correlations. The feature at ∼3.5 Å was best fit by 2 Gaussian functions constrained to have the same width with centers at 3.25 Å and 3.47 Å. As the dominant Al species in as-prepared MACC, the Cl···Cl pairs in the $AlCl_4^-$ tetrahedron will have strong contributions to this broad feature, likely associated with the 3.47 Å feature based on comparison to the $AlCl_4^-$ in the solid state with Cl···Cl distance of 3.42 Å, (the simulated PDF of $AlCl_4^-$ can be found in Figure S2). The remaining 3.25 Å feature must be associated with the Mg complexes, and can be attributed to next-nearest neighbor distances.

To further interpret the possible next-nearest neighbor correlations that dominate around 3.3 Å in Mg complexes, the PDF of several possible structures were simulated using PDFgui (Figure S1). The structures used to simulate the PDFs are the stable complexes predicted by Wan and Prendergast.[44] In the experimental data, the first shell correlations of the Mg complexes appear at 2.37 Å. This correlation can be used to compare the simulated PDF patterns with the experimental data. In this respect, the 3.3 Å peak in the experimental data is significantly more intense than the contributions from the first shell correlations associated with Mg. Interestingly, the only coordination environment in which the 3.3 Å peak appears with significant intensity compared to the first shell correlations in the simulated complexes is that associated with octahedral Mg (Figure S1f). In octahedral Mg, a peak in the PDF at 3.3 Å is due to the pairwise correlations on the edge of the octahedron including strongly scattering Cl atoms, Cl−Cl and Cl−O. Lower coordination numbers, such as the pentacoordinate case, result in a lower intensity of Cl−O correlations and a broader, less intense peak in the 3.3 Å region. Octahedral coordination strongly implicates dimeric Mg since the monomeric Mg complexes are predicted to be tetrahedral.[44,48] The only dimeric Mg complex in which Mg is octahedrally coordinated is that with 3 bridging Cl,[44] thus implicating the $[Mg_2(\mu\text{−}Cl)_3\cdot 6THF]^+$. This analysis agrees well with the prediction that Mg must be cationic in the as-prepared MACC due to the high concentration of anionic $AlCl_4^-$. Further evidence suggesting a dimeric Mg structure comes from the ^{35}Cl NMR data which shows a deshielding of the Cl bound to Mg complexes in the MACC relative to that in the $MgCl_2$ solution. The slight deshielding could be due to the formation of a Mg dimer through bridging Cl. The presence of an octahedral Mg dimer is consistent with previous experimental work that infers the presence of a six-coordinate Mg dimer in the MACC system in glyme solvents.[31] However, the $[Mg_2(\mu\text{−}Cl)_3\cdot 6THF]^+$ complex is predicted to be unstable according to the calculations.[44,48] Therefore, the dimer must be stabilized in the as-prepared MACC solution compared to a solution containing only Mg complexes, such as those simulated.[44] We suggest that counterions present in the as-prepared MACC play a significant role in stabilizing the Mg dimer.

The conditioned MACC exhibits correlations at distances similar to those found in the as-prepared MACC. However, the relative contribution of each correlation changes significantly. In the first shell region of the conditioned MACC (2−3 Å), the intensity of the Mg−Cl correlation at 2.39 Å increases significantly while the Al−Cl correlation at 2.15 Å decreases relative to the as-prepared case. The decrease of Al first shell correlation intensity agrees well with the previous work showing Al is irreversibly deposited during conditioning[14] and the ^{27}Al NMR data that shows a decrease in concentration of Al species. The increase in Mg first shell correlations could be due to either an increase in the coordination number of the Mg or an increase in Mg concentration. The increase in Mg concentration is much more likely considering Mg oxidation must occur at the Mg counter electrode as a result of Al deposition. We suggested above that coordination of Mg in the as-prepared solution is octahedral; further increases in coordination number to the Mg would be very unlikely.

In the second sphere region, the correlation at 3.27 Å increases in intensity in the conditioned MACC relative to the

DOI: 10.1021/jacs.5b10987
J. Am. Chem. Soc. 2016, 138, 328−337

as-prepared while the 3.49 Å correlation decreases. The 3.49 Å correlation is ascribed to Cl−Cl correlations in $AlCl_4^-$ tetrahedron and the lower magnitude in the as-prepared MACC agrees nicely with the ^{27}Al NMR that clearly shows a decrease in $AlCl_4^-$ concentration. Additionally, the decrease in the 3.49 Å intensity is commensurate with the decrease in the 2.15 Å correlation ascribed to Al first shell correlations, further confirming the suggested assignments. Because the $AlCl_4^-$ concentration decreases in the conditioned MACC, the increase in the 3.27 Å peak cannot be due to Al complexes and thus the assignment of this peak to Mg complexes, as described previously, is further confirmed. Additionally, the intensity of the 3.27 Å peak increases commensurately with the intensity of Mg first shell correlations at 2.39 Å. The position of this second sphere correlation again suggests octahedral Mg in the conditioned MACC, which again implicates the Mg dimer $[Mg_2(\mu{-}Cl)_3{\cdot}6THF]^+$. The concentration of the $[Mg_2(\mu{-}Cl)_3{\cdot}6THF]^+$ in the conditioned MACC must be much greater than the as-prepared MACC due to the increase in intensity of the 3.27 Å correlation.

Discussion of Conditioning Mechanism. Using the data from the multitechnique characterization of the MACC electrolyte, we propose a mechanism describing the MACC in the as-prepared and conditioned states (Figure 7). The as-

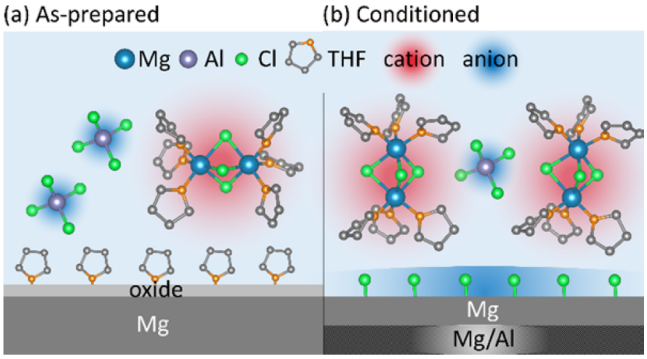

Figure 7. Scheme depicting the speciation in the MACC electrolyte solution (a) as-prepared and (b) conditioned as determined by Raman, SERS, NMR, and PDF data. The conditioning process irreversibly electrodeposits Al resulting in a decrease in $AlCl_4^-$ concentration, an increase in $[Mg_2(\mu{-}Cl)_3{\cdot}6THF]^+$ concentration, and the formation of Cl^-. Cl^- decorates the electrode surface and promotes Mg electrodeposition. Please note that stoichiometry is not preserved in this schematic.

prepared MACC is not a simple combination of the component $MgCl_2$ and $AlCl_3$ solutions. Instead, the addition of the two cations allows Al to form $AlCl_4^-$, as evidenced by ^{27}Al NMR and Raman, and this anion must be charge balanced by cationic Mg. The cationic Mg complexes are very likely $[Mg_2(\mu{-}Cl)_3{\cdot}6THF]^+$ as evidenced by a strong contribution in the PDF that implicates octahedral Mg. Additionally, the ^{35}Cl NMR shows a slight deshielding of the Cl environment in the as-prepared solution compared to the $MgCl_2$ solution which is nicely explained by a terminal Cl conversion to a bridging Cl. The presence of the dimeric Mg complex is completely consistent with the stoichiometry of the as-prepared solution. Thus, the as-prepared MACC can be described as

$$AlCl_3{\cdot}2THF + 2MgCl_2 + 4THF \rightarrow AlCl_4^- + [Mg_2(\mu{-}Cl)_3{\cdot}6THF]^+ \quad (1)$$

Integration of the ^{35}Cl NMR data measured for the as-prepared MACC confirms eq 1. The Mg-associated Cl integrates to 41% of the Cl signal while the Al-associated Cl integrates to 59% of the signal (eq 1 would result in values of 43% and 57%, respectively). The small deviation from the theoretical value is an indication of some mixed speciation present in the solution.

Upon conditioning the as-prepared MACC, Al is irreversibly deposited during the cathodic sweep[14] resulting in an increase in the concentration of Mg^{2+} via oxidation of the counter electrode. Some Al remains in solution as $AlCl_4^-$, as determined by the ^{27}Al NMR and Raman. In the conditioned MACC, more Cl is present bound to Mg than Al relative to the as-prepared solution suggesting Mg species formed by counter electrode oxidation contain Cl ligands. Both the as-prepared and conditioned MACC exhibit similar Cl chemical shifts suggesting the Cl environment in the Mg complexes in the conditioned MACC is similar to that found in the as-prepared. Additionally, an increase in intensity in the correlation that implicates octahedral Mg is observed in the PDF as a result of conditioning. Thus, the condition process results in the formation of a higher concentration of octrahedral Mg complexes that contain Cl in a similar environment to that of the as-prepared solution. This analysis implicates the presence of $[Mg_2(\mu{-}Cl)_3{\cdot}6THF]^+$ in the conditioned MACC. Previous studies have implicated the Mg dimer as the active Mg species in a variety of Mg electrolytes that contain Cl, including $MgCl_2$-$AlEtCl_2$,[13] $MgCl_2$-$AlPh_3$,[13,49] and HMDSMgCl-$AlCl_3$,[S1] however, the evidence for the Mg dimer is largely found in solid state structures with little evidence for its presence in solution.

We next address a mechanism whereby Al could be deposited, Mg^{2+} liberated from the counter and additional $[Mg_2(\mu{-}Cl)_3{\cdot}6THF]^+$ formed. One such reaction could be

$$4AlCl_4^- + 6Mg_{(s)} \rightarrow 4Al_{(s)} + 3[Mg_2(\mu{-}Cl)_3{\cdot}6THF]^+ + 7Cl^- \quad (2)$$

Data that supports irreversible Al deposition as a result of the conditioning process includes (a) the presence of Al on the electrode surface following conditioning,[14] (b) substantial cathodic current at voltages corresponding to those expected for Al electrodeposition, i.e., above 0 V vs Mg, during the initial conditioning cycles, (c) increase in the Mg:Al ratio from 2:1 to 2.6:1,[14] and (d) quantitative evidence of Al depletion from the solution by ^{27}Al NMR. It is important to note that although Al electrodeposition occurs during the conditioning process, Al electrodeposition eventually terminates as evidenced by the lack of Al on fresh electrodes used for Mg electrodeposition in conditioned MACC.[14] Although Al deposition has ceased, Al species including $AlCl_4^-$ remain in the solution as determined by ICP,[14] ^{27}Al NMR, and Raman. Although Al reduction results in a change in the composition of the electrode (as indicated in Figure 7), the plated Al has no effect on the ability of the MACC to deposit Mg.[14] Once MACC is conditioned, a clean Pt electrode exhibits the same electrodeposition overpotential and Coulombic efficiencies as the Pt electrode used to condition the MACC.[14] Deposition of $4Al^{3+}$ must result in the formation of 3 Mg dimers, i.e., 6 Mg^{2+}, due to the difference in oxidation state of the two cations. The counterion that forms

DOI: 10.1021/jacs.5b10987
J. Am. Chem. Soc. 2016, 138, 328−337

as a result of Al reduction and Mg oxidation is suggested to be free Cl^- in equation 2.

Indeed, evidence for free Cl^- is observed in the SERS spectrum of the conditioned MACC and, as expected, is absent in the as-prepared MACC. Further evidence for Cl^- would be expected in the ^{35}Cl NMR. To determine the shift of Cl^- in THF, the ^{35}Cl NMR of a LiCl solution in THF was measured and, as expected, a sharp peak is observed around 0 ppm (Figure S3). However, the sharp Cl^- signal near 0 ppm that would further confirm Cl^- in the conditioned MACC is notably absent from the ^{35}Cl NMR. The lack of Cl^- signal in the NMR could be due to fast exchange between the Cl^- and Al or Mg complexes, likely with $AlCl_4^-$,[37] resulting in only two observable resonances in the spectrum. In fact, the ^{35}Cl signal associated with Al is broader in the conditioned electrolyte which could be due to exchange with Cl^-. Alternatively, the solvation structure of the Cl^- could cause a broad resonance that is hidden beneath the observed signals. In order to decouple exchange, solutions are commonly cooled or the concentration of the analyte is decreased, however, neither methodology can be used in this case due to the sensitivity of the complex equilibria in the conditioned MACC on both temperature and concentration.

We suggest that the Mg dimer is present in both the as-prepared and the conditioned MACC solutions. The combination of a high concentration of the Mg dimer and the formation of free Cl^- as a result of Al deposition enhances the Mg electrodeposition. SERS shows that as-prepared MACC results in a THF decorated surface, which is likely extremely passivating due to the high oxophilicty of Mg,[35,36] while the conditioned MACC forms a Cl decorated surface. Although the SERS experiments were performed on a Cu substrate to provide the SERS enhancement, the detected free Cl^- is expected to readily adsorb on Mg surfaces as this process is predicted to be highly exothermic.[50] The crucial role of Cl^- in the electrodeposition of multivalent cations is not unprecedented. In fact, Cl^- plays a major role in enhancing the Mg electrodeposition kinetics in the $PhMgCl/AlCl_3$ electrolyte.[52] Additionally, Cl^- is well-known to enhance the electrodeposition of Cu[53] and Fe.[54] In the Cu case, for example, Cl^- is adsorbed on the electrode surface catalyzes the $Cu^{2+} \rightarrow Cu^+$ electron transfer by stabilizing the Cu^+ intermediate.[53]

The shift in bulk speciation as a result of conditioning is the cause for enhanced Mg electrodeposition. Changes in the electrode composition itself as a result of Al reduction do not contribute to the performance of the electrolyte as evidenced by the same Coulombic efficiencies and electrodeposition overpotentials achieved by a clean electrode in the conditioned MACC.[14] Additionally, it is important to note that removal of electrolyte solution contaminants may occur during the conditioning process, however, contaminant removal is not the main factor attributing to the electrolyte performance. First, contaminates are not observed in the as-prepared solution by ^{27}Al NMR, ^{35}Cl NMR, or Raman spectroscopy. Second, if removal of contaminants as a result of conditioning were the main cause for enhanced Mg electrodeposition, then the MACC electrolyte should maintain its activity over time. Instead, we observe aging as the electrolyte rests that can be explained by the equilibration of the Cl^- with Al and Mg species in solution due the instability of Cl^- in THF in addition to previously observed poly-THF formation.[14]

CONCLUSION

The MACC is a complex system that requires a multitechnique characterization approach to understand the speciation of Mg and Al in the active state. Bulk speciation of the Al shifts significantly as a result of conditioning which results in an increase in the concentration of cationic, octahedral Mg. Octahedral coordination implicates the Mg dimer $[Mg_2(\mu\text{-}Cl)_3{\cdot}6THF]^+$. Although conditioning increases the concentration of the dimer, we have shown that $[Mg_2(\mu\text{-}Cl)_3{\cdot}6THF]^+$ is also present in the as-prepared electrolyte. The enhanced Mg electrodeposition occurs by virtue of increasing the concentration of the dimer in conjunction with formation of free Cl^- in solution. The presence of excess Cl^- has previously been associated with enhanced Mg electrodeposition.[52] The exact role of Cl^- is not completely clear; however, Cl^- is likely useful in depassivating the electrode to allow Mg deposition.

Here, we have shown that the equilibria responsible for creating the active MACC electrolyte are extremely complicated and are affected by all components, including the solvent. The dependence of the Mg electrochemical activity on the speciation of the bulk electrolyte has important implications in designing Mg electrolytes.

ASSOCIATED CONTENT

Supporting Information

The Supporting Information is available free of charge on the ACS Publications website at DOI: 10.1021/jacs.5b10987.

Tabulated fit parameters from the Gaussian fits of the PDF data, PDF calculations of possible Mg complexes, PDF calculations of $AlCl_4^-$ and $[Mg_2(\mu\text{-}Cl)_3{\cdot}6THF]^+$, and ^{35}Cl NMR of LiCl and TBACl in THF. (PDF)

AUTHOR INFORMATION

Corresponding Authors

*chapmank@aps.anl.gov
*agewirth@illinois.edu

Notes

The authors declare no competing financial interest.

ACKNOWLEDGMENTS

This work was supported as part of the Joint Center for Energy Storage Research, an Energy Innovation Hub funded by the U.S. Department of Energy, Office of Science, Basic Energy Sciences. Work done at Argonne and use of the Advanced Photon Source, an Office of Science User Facility operated for the U.S. Department of Energy Office of Science by Argonne National Laboratory, were supported by the U.S. Department of Energy under Contract No. DE-AC02-06CH11357. K. A. S acknowledges postdoctoral funding from the St. Elmo Brady Future Faculty Fellowship. C. J. B. acknowledges a National Science Foundation Graduate Research Fellowship (No. NSF DGE-1144245) and a Springborn Fellowship. The authors thank Liwen F. Wan and David Prendergast for helpful discussions and providing cif files of the Mg complexes. The authors acknowledge Saul H. Lapidus for helpful discussions, Tim T. Fister for assistance with electrochemical equipment at the APS, Niya Sa for assistance with materials at the ANL, and Kevin G. Schmitt for helpful discussion regarding Raman results.

DOI: 10.1021/jacs.5b10987
J. Am. Chem. Soc. 2016, 138, 328−337

REFERENCES

(1) Aurbach, D.; Lu, Z.; Schechter, A.; Gofer, Y.; Gizbar, H.; Turgeman, R.; Cohen, Y.; Moshkovich, M.; Levi, E. *Nature* **2000**, *407*, 724−727.
(2) Matsui, M. *J. Power Sources* **2011**, *196*, 7048−7055.
(3) Aurbach, D.; Cohen, Y.; Moshkovich, M. *Electrochem. Solid-State Lett.* **2001**, *4*, A113−A116.
(4) Liebenow, C.; Yang, Z.; Lobitz, P. *Electrochem. Commun.* **2000**, *2*, 641−645.
(5) Vestfried, Y.; Chusid, O.; Goffer, Y.; Aped, P.; Aurbach, D. *Organometallics* **2007**, *26*, 3130−3137.
(6) Pour, N.; Gofer, Y.; Major, D. T.; Aurbach, D. *J. Am. Chem. Soc.* **2011**, *133*, 6270−6278.
(7) Mohtadi, R.; Matsui, M.; Arthur, T. S.; Hwang, S.-J. *Angew. Chem., Int. Ed.* **2012**, *51* (39), 9780−9783.
(8) Carter, T. J.; Mohtadi, R.; Arthur, T. S.; Mizuno, F.; Zhang, R.; Shirai, S.; Kampf, J. W. *Angew. Chem., Int. Ed.* **2014**, *53* (12), 3173−3177.
(9) Tutusaus, O.; Mohtadi, R.; Arthur, T. S.; Mizuno, F.; Nelson, E. G.; Sevryugina, Y. V. *Angew. Chem., Int. Ed.* **2015**, *54*, 7900−7904.
(10) Ha, S.-Y.; Lee, Y.-W.; Woo, S. W.; Koo, B.; Kim, J.-S.; Cho, J.; Lee, K. T.; Choi, N.-S. *ACS Appl. Mater. Interfaces* **2014**, *6*, 4063−4073.
(11) Shterenberg, I.; Salama, M.; Yoo, H. D.; Gofer, Y.; Park, J.-B.; Sun, Y.-K.; Aurbach, D. *J. Electrochem. Soc.* **2015**, *162*, A7118−A7128.
(12) Doe, R. E.; Han, R.; Hwang, J.; Gmitter, A. J.; Shterenberg, I.; Yoo, H. D.; Pour, N.; Aurbach, D. *Chem. Commun.* **2013**, *50*, 243−245.
(13) Liu, T.; Shao, Y.; Li, G.; Gu, M.; Hu, J.; Xu, S.; Nie, Z.; Chen, X.; Wang, C.; Liu, J. *J. Mater. Chem. A* **2014**, *2*, 3430−3438.
(14) Barile, C. J.; Barile, E. C.; Zavadil, K. R.; Nuzzo, R. G.; Gewirth, A. A. *J. Phys. Chem. C* **2014**, *118*, 27623−27630.
(15) Oberst, J. L.; Jhong, H.-R.; Kenis, P. J. A.; Gewirth, A. A. *J. Solid State Electrochem.* **2015**, 1−6.
(16) Chupas, P. J.; Chapman, K. W.; Lee, P. L. *J. Appl. Crystallogr.* **2007**, *40*, 463−470.
(17) Chupas, P. J.; Qiu, X.; Hanson, J. C.; Lee, P. L.; Grey, C. P.; Billinge, S. J. L. *J. Appl. Crystallogr.* **2003**, *36*, 1342−1347.
(18) Qiu, X.; Thompson, J. W.; Billinge, S. J. L. *J. Appl. Crystallogr.* **2004**, *37*, 678−678.
(19) Handlíř, K.; Holeček, J.; Beneš, L. *Collect. Czech. Chem. Commun.* **1985**, *50*, 2422−2430.
(20) Øye, H. A.; Rytter, E.; Klæboe, P.; Cyvin, S. J.; Lagerlund, I.; Ehrenberg, L. *Acta Chem. Scand.* **1971**, *25*, 559−576.
(21) Balasubrahmanyam, K.; Nanis, L. *J. Chem. Phys.* **1965**, *42*, 676−680.
(22) Alves, C. C.; Campos, T. B. C.; Alves, W. A. *Spectrochim. Acta, Part A* **2012**, *97*, 1085−1088.
(23) Capwell, R. J. *Chem. Phys. Lett.* **1972**, *12*, 443−446.
(24) Gallinella, E.; Cadiolia, B.; Pierre Flament, J.; Berthier, G. *J. Mol. Struct.: THEOCHEM* **1994**, *315*, 137−148.
(25) Cadioli, B.; Gallinella, E.; Coulombeau, C.; Jobic, H.; Berthier, G. *J. Phys. Chem.* **1993**, *97*, 7844−7856.
(26) Derouault, J.; Granger, P.; Forel, M. T. *Inorg. Chem.* **1977**, *16*, 3214−3218.
(27) Ojha, A. K.; Srivastava, S. K.; Peica, N.; Schlücker, S.; Kiefer, W.; Asthana, B. P. *J. Mol. Struct.* **2005**, *735*−*736*, 349−357.
(28) Benevenuto, R. L.; Alves, W. A. *J. Raman Spectrosc.* **2008**, *39*, 490−494.
(29) Ojha, A. K.; Srivastava, S. K.; Peica, N.; Schlücker, S.; Kiefer, W.; Asthana, B. P. *J. Mol. Struct.* **2005**, *735*−*736*, 349−357.
(30) Alves, C. C. *Spectrochim. Acta, Part A* **2012**, *97*, 1085−1088.
(31) Barile, C. J.; Nuzzo, R. G.; Gewirth, A. A. *J. Phys. Chem. C* **2015**, *119*, 13524−13534.
(32) Feng, Z. V.; Li, X.; Gewirth, A. A. *J. Phys. Chem. B* **2003**, *107*, 9415−9423.
(33) Brown, G. M.; Hope, G. A. *J. Electroanal. Chem.* **1996**, *413*, 153−160.
(34) Niaura, G.; Malinauskas, A. *Chem. Phys. Lett.* **1993**, *207*, 455−460.
(35) Ghijsen, J.; Namba, H.; Thiry, P. A.; Pireaux, J. J.; Caudano, P. *Appl. Surf. Sci.* **1981**, *8*, 397−411.
(36) Thiry, P. A.; Ghijsen, J.; Sporken, R.; Pireaux, J. J.; Johnson, R. L.; Caudano, R. *Phys. Rev. B: Condens. Matter Mater. Phys.* **1989**, *39*, 3620−3631.
(37) Nöth, H.; Rurländer, R.; Wolfgardt, P. *Z. Naturforsch., B: J. Chem. Sci.* **1982**, *37*, 29−37.
(38) Lefebvre, M. C.; Conway, B. E. *J. Electroanal. Chem.* **1998**, *448*, 217−227.
(39) Benn, R.; Rufińska, A.; Lehmkuhl, H.; Janssen, E.; Krüger, C. *Angew. Chem., Int. Ed. Engl.* **1983**, *22*, 779−780.
(40) Kidd, R. G.; Truax, D. R. *J. Am. Chem. Soc.* **1968**, *90*, 6867−6869.
(41) Couch, D. E.; Brenner, A. *J. Electrochem. Soc.* **1952**, *99*, 234−244.
(42) Mizrahi, O.; Amir, N.; Pollak, E.; Chusid, O.; Marks, V.; Gottlieb, H.; Larush, L.; Zinigrad, E.; Aurbach, D. *J. Electrochem. Soc.* **2008**, *155*, A103−A109.
(43) Gray, J. L.; Maciel, G. E. *J. Am. Chem. Soc.* **1981**, *103*, 7147−7151.
(44) Wan, L. F.; Prendergast, D. *J. Am. Chem. Soc.* **2014**, *136*, 14456−14464.
(45) Partin, D. E.; O'Keeffe, M. *J. Solid State Chem.* **1991**, *95*, 176−183.
(46) Tsirelson, V. G.; Avilov, A. S.; Abramov, Y. A.; Belokoneva, E. L.; Kitaneh, R.; Feil, D. *Acta Crystallogr., Sect. B: Struct. Sci.* **1998**, *54*, 8−17.
(47) Cowley, A. H.; Cushner, M. C.; Davis, R. E.; Riley, P. E. *Inorg. Chem.* **1981**, *20*, 1179−1181.
(48) Canepa, P.; Jayaraman, S.; Cheng, L.; Raiput, N. N.; Richards, W. D.; Gautam, G. S.; Curtiss, L. A.; Persson, K. A.; Ceder, G. *Energy Environ. Sci.* **2015**, *8*, 3718−3730.
(49) Liu, T.; Cox, J. T.; Hu, D.; Deng, X.; Hu, J.; Hu, M. Y.; Xiao, J.; Shao, Y.; Tang, K.; Liu, J. *Chem. Commun.* **2015**, *51*, 2312−2315.
(50) Canepa, P.; Gautam, G. S.; Malik, R.; Jayaraman, S.; Rong, Z.; Zavadil, K. R.; Persson, K.; Ceder, G. *Chem. Mater.* **2015**, *27*, 3317−3325.
(51) Kim, H. S.; Arthur, T. S.; Allred, G. D.; Zajicek, J.; Newman, J. G.; Rodnyansky, A. E.; Oliver, A. G.; Boggess, W. C.; Muldoon, J. *Nat. Commun.* **2011**, *2*, 427.
(52) Esbenshade, J. L.; Barile, C. J.; Fister, T. T.; Bassett, K. L.; Fenter, P.; Nuzzo, R. G.; Gewirth, A. A. *J. Phys. Chem. C* **2015**, *119*, 23366−23372.
(53) Nagy, Z. *J. Electrochem. Soc.* **1995**, *142*, L87.
(54) Johnson, D. C.; Resnick, E. W. *Anal. Chem.* **1977**, *49*, 1918−1924.

DOI: 10.1021/jacs.5b10987
J. Am. Chem. Soc. 2016, 138, 328−337